ON THE ESTIMATION OF ENERGY LOSSES FROM MUNICIPAL HEATING NETWORKS USING IR-THERMOGRAPHY

Sune R. J. Axelsson

Linköping University
Department of Electrical Engineering
S-581 83 Linköping
Sweden
Commission VII

ABSTRACT

This paper describes a computer model for the prediction of surface temperature profiles over district heating lines. Algorithms are suggested for quantitative estimation of energy losses and insulation conditions from thermal-IR imagery. Main limitations of the technique and the choice of favourable conditions for the data acquisition are analysed.

1 INTRODUCTION

Airborne and ground-based IR-thermography has been identified as a useful instrument for the detection of energy losses from buildings and district heating networks, see e.g. [1]-[3]. The accuracy of the technique and the optimum conditions of the data acquisition need further investigations, however.

In this paper, a computer model will first be described for predictions of the heat flux and temperature field around a buried heating line. Algorithms are then derived for the estimation of energy losses using thermal-IR imagery as input. Various error sources and their influence upon the accuracy are analyzed and discussed.

2 PHYSICAL BACKGROUND

The temperature field $T(x,y,z;t)$ and heat flux $Q(x,y,z;t)$ in the ground can be estimated from

$$Q = - \lambda \, \mathrm{grad}(T) \qquad (1.a)$$

$$\mathrm{div}(Q) = - C \frac{dT}{dt} \qquad (1.b)$$

where λ is the thermal conductivity and C is the heat capacity per unit volume.

For the analysis of district heating networks with near-homogeneous conditions along the line, a two-dimensional version of (1) can be applied.

The boundary conditions of (1) are defined by the water temperature inside the tubes and the heat exchange at the ground surface

$$Q(0,y,z;t) = I(1-A) + \varepsilon\sigma[T_e^4-T^4]-H-LE \qquad (2)$$

where I is the short-wave irradiance, A is the albedo of the ground surface, ε is its long-wave emissivity, σ is the Stefan-Bolzmann constant, T is the surface temperature, H is the sensible heat flux, LE is the latent heat flux, and T_e is the blackbody temperature of the incident long-wave radiation from the upper hemisphere including the contribution from neighbouring objects like trees, buildings and hedges.

The sensible heat flux of (2) is described by

$$H = k_o(T - T_o) \qquad (3)$$

where T_o is the air-temperature.

The factor k_o is highly influenced by windspeed, but the surface roughness and atmospheric stability have also significant effects. An improved estimate of k_o can be obtained using the Monin-Obukhov scaling theory with meteorological data as input [5] - [6].

The latent heat flux (LE), which highly influences the temperature of wet and semi-dry surfaces, is defined by

$$LE = k_o(L/C_p)[hX(T)-h_oX(T_o)] \qquad (4)$$

where h_o represents the relative humidity of the air at reference height, h is the corresponding value at the surface, L is the latent heat of vaporization, C_p is the specific heat of dry air at constant pressure, and X(T) is the saturation mixing ratio.

3 FINITE DIFFERENCE MODEL

The temperature field around the heating line can be estimated under very general conditions by using the method of finite differences [4], [7].

The top-layer of ground is then divided into a number of small volume elements to the depth $D=N_1d$ and width $B=M_1d$. For a two-dimensional model, the extension of the elements is d in the x- and y-directions and unit length along the heating line (z). Before the start of the simulation, the thermal conductivity $\lambda(n,m)$ and heat capacity per unit volume C(n,m) are defined for the total region: $1 < n < N_1$ and $1 < m < M_1$.

For a new time-step $t=(k+1)\Delta t$, the inflow of heat (W) to a volume element (n,m) is computed using

$$Q_s(n,m,k+1) = Q(1)+Q(2)+Q(3)+Q(4) \qquad (5)$$

where Q(k) are heat fluxes from adjacent elements.

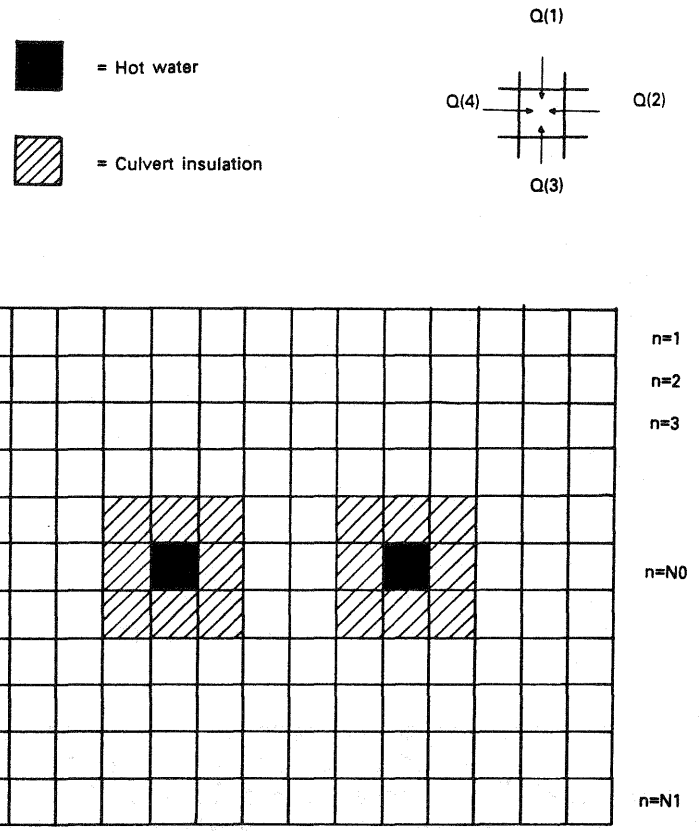

FIGURE 1. Finite difference model.

The temperature of the subvolume (n,m) is updated for $t=(k+1)\Delta t$ using the following algorithm derived from (1.b)

$$T(n,m,k+1) = T(n,m,k) + Q_{sa}(n,m)\Delta t/[C(n,m)d^2]$$

$$Q_{sa}(n,m) = [Q_s(n,m,k+1) + Q_s(n,m,k)]/2 \qquad (6)$$

where $Q_{sa}(n,m)$ represents the average heat flow into the volume (n,m) during the time-step Δt.

At the surface boundary (n = 1), Q(1) in (5) is determined by the heat exchange at the ground/air interface. From (1.a) and the use of a linear approximation of (2) about T_o, Q(1) can be described as

$$Q(1) = d\lambda(1,m)[T_s - T(1,m,k)]/(d/2) \qquad (7a)$$

$$Q(1) = d[k_1(T_o - T_s) + Q_o] \qquad (7b)$$

where T_s is the surface temperature, T_o is the air-temperature and

$$Q_o = I(1-A) + \varepsilon\sigma[T_e^4 - T_o^4] - LE(T_o)$$

$$k_1 = k_o + 4\varepsilon\sigma T_o^3 + \left.\frac{\delta(LE)}{\delta T}\right|_{T=T_o} \qquad (8)$$

From (7), the two variables Q(1) and T_s of the volume (1,m) are now easily solved.

When the above algorithms have been applied for all the elements, the whole procedure is repeated for new time steps. For further material, see reference [4] or [8].

By using the finite difference model described above a set of surface temperature profiles across a district heating line was generated for different conditions, see Figures 2 - 7.

As a reference case was used two heating pipes buried 1.1 m below the ground surface (measured from the symmetry axis), with an inner diameter of 0.2 m and covered by 0.2 m thick layers of insulation (Fig. 1). The thermal conductivity of soil and insulation materials were 1.5 and 0.5 W/m^2K, respectively, giving heat losses of about 200 W per metre length. The hot water temperatures of the two pipes were 100 and 60°C, which explains the slight unsymmetry of the temperature profiles. A spatial resolution of 0.2 m, dry surface conditions (LE=0) and a soil temperature of 7°C were also assumed. In general, the graphs represent profiles 360 hours after the start of the simulation.

In order to reduce the number of parameters to be varied, the boundary condition of (7)-(8) with Q_0=0 and constant k_1 during the day were applied. It was shown that the diurnal variations of Q_0 due to changes in sun radiation, air temperature and sky temperature do not affect the thermal contrast of the heating line area, if homogeneous ground cover and linearized boundary conditions can be applied [4]. However, diurnal changes of k_1 or k_0 due to varying wind-speed or surface humidity make the boundary condition (7b) non-linear, giving a significant change of the temperature contrast.

Figure 2 shows temperature profiles derived for three heating lines with great differences with respect to the thermal insulation: λ=0.05, 0.15 and 0.5 W/mK. The corresponding total heat losses are 34, 90 and 210 W/m, respectively. The thermal contrasts at the surface are 0.7, 1.8 and 4.3 K, which means a calibration factor of about 50 W/mK.

4 HEAT LOSS ESTIMATION ALGORITHMS

A significant temperature contrast is mostly observed over district heating lines as a result of the enhanced soil heat flux. From (2), the upward heat flux increase at surface level is

$$\Delta Q = H-H_1+LE-LE_1+I_1(1-A_1)-I(1-A)+\varepsilon_1\sigma T_{e1}^4- \\ -\varepsilon\sigma T_e^4+\varepsilon\sigma T^4-\varepsilon_1\sigma T_1^4. \qquad (9)$$

where index 1 denotes background conditions.

For homogeneous radiation exposure and surface cover ($I=I_1$, $A=A_1$, $T_e=T_{e1}$ and $\varepsilon=\varepsilon_1$)

$$\Delta Q = H-H_1+LE-LE_1+\varepsilon\sigma[T^4-T_1^4]. \qquad (10)$$

If wind-speed (k_0) and surface humidity (h) are similar as well, we can rewrite (10) using linear approximations of LE and the long-wave sky radiation about the surface temperature of the background (T_1)

$$\Delta Q = k_1(T - T_1) \tag{11}$$

where k_1 is defined by (8).

Typical values of k_0 is 5 - 10 W/m^2K at calm weather. For dry surface conditions, the latent heat term of k_1 can be neglected. If T_1=285 K and ε=0.95, for instance, $k_1=5+k_0$ is obtained.

From (11), the increased heat flux to the atmosphere over the heating line area (ΔQ) is proportional to the temperature contrast $\Delta T = T - T_1$. The increase of the heat flow to the atmosphere per unit length of the heating line (W/m) is predicted by integrating ΔQ across the line

$$\Delta Q_0 = k_1 \int_{-\infty}^{\infty} (T(x) - T_1)dx \tag{12}$$

The total increase of the surface heat flow (W) through a limited area is estimated from (12) by integrating as well in the z-direction.

Under favourable conditions

$$Q_L = F_1 \Delta Q_0 = F_1 k_1 \int_{-\infty}^{\infty} (T(x) - T_1)dx \tag{13}$$

should be a useful estimator of the total heat losses of the heating line (W/m). The factor F_1 is calibrated from field experiments or by running the simulation model described above. The simulation results indicate that F_1 mostly is in the range 1.5 - 2.5 for near-stable conditions.

A simplified and more approximative prediction algorithm is as follows

$$Q_L' = F_2 \Delta T \tag{14}$$

i.e. direct proportionality between heat-losses and surface temperature contrast.

Obviously, the heat losses from the district heating network can also be estimated using more conventional metods e.g. by comparing the thermal-IR contrasts with those obtained over reference culverts with well-defined insulating performance.

The method can be further improved, if the heating line contrasts observed in the IR-imagery are subdivided into different classes depending on the type of ground cover e.g. bare soil, asphalt, grass cover. A statistical analysis of the temperature contrasts of the different terrain classes will point out those representing enhanced heat losses.

5 LIMITATIONS

From the preceding analysis, it was obvious that there are several limitations, which reduce the accuracy of the estimation algorithms. A main assumption was the similarity as regards albedo, emissivity, surface humidity, inclination, wind speed, surface roughness, radiation exposure and thermal inertia. Local variations of these parameters can generate both false background contrasts and give an increased error at the heat loss estimation.

Simulation results for an October day with low wind-speed and overcast sky [4] showed that typical variations of albedo, emissivity and the thermal inertia will generate contrasts of about 0.4 K at noon and 0.1-0.2 K in the night. For F_2=50 W/mK, these contrasts correspond to energy losses of 20 and 5-10 W/m respectively.

Local variations in wind-speed (k_0) and sky temperature (T_e) will further reduce the sensitivity of the estimation procedure [4]. Figure 3 shows that the thermal contrast is reduced about 1.3 K at a location, where k_0=10 instead of 5 W/m^{2}K (reference value). The energy losses of the heating line are not very affected by the actual k_0-value, however, which means 30 % error when (12)-(13) and the calibration constant k_0=5 W/m^{2}K are applied.

Extended algorithms [4] based upon (9)-(10) compensate for the above parameter deviations, but errors in modelling and parameter estimation will reduce the accuracy of the procedure.

The estimation error is highly increased at non-stable conditions. This effect is clearly displayed by Figure 4, showing profiles 72, 360 and 1200 hours after the start of the simulation, which is equivalent to a change of the conductivity of the insulation from zero to 0.5 W/mK. Graphs of the time variations of the energy losses (Q_L) and the heat flux increase at the surface (ΔQ_0) during t=0 to 1200 hours are shown in Figure 5. Obviously, there is a time delay of a week or more until the temperature profiles are approaching near-stable conditions. Hence, recent subsurface energy leaks are not easily detected and estimated using IR-thermography.

Furthermore, the simulation results of [4] showed that the accuracy of the estimation is reduced when k_0 or k_1 are time-varying. Diurnal variations of k_0 between 5 and 10 W/m^{2}K made the heat flux contrast vary between 93 and 115 W/m giving an error of 10% at the heat loss estimation. The diurnal variations of air-temperature, sky temperature and solar radiation did not give any significant reduction of the accuracy, however.

Large estimation errors can also be generated by unpredictable variations of culvert depth. From Fig. 6 the thermal contrast is reduced two degrees when the depth of the pipes (measured from the centre) is increased from 0.9 m to 1.3 m. Since the heat losses are only slightly modified (from 215 to 206 W/m), the factors F_1 and F_2 of (15) and (16) should be increased 60 per cent to give a correct heat loss estimate.

The thermal conductivity of the soil is also varying due to differences in water content, soil composition and density. Figure 7 shows for the reference culvert that a changed soil conductivity from 1.5 to 1.0 W/mK will reduce the temperature contrast 0.6 K. Simultaneously, the heat loss of the heating line is changed from 210 to 175 W/mK. The estimation procedure (14) predicts 185 W/m when calibrated for the reference case. Hence, variations in soil conductivity give only a minor reduction of the accuracy of (13) and (14).

The influence of tube depth, tube insulation, k_0 and soil conductivity upon the factor F_1 of the estimation algorithm is summarized in Fig. 8, which shows the relationship between the total heat losses Q_1 and ΔQ_0 for the parameter variation of Figures 2, 3, 6 and 7 and three different times after the start of the simulation (144, 240 and 360 hours). Figure 8 indicates that the calibration constant F_1 is varying between 1.8 and 4.4, mostly as a result of transient effects. If we restrict the samples to t = 360 hours, the range of variation is reduced to 1.8 - 2.3.

The corresponding relationship between the total heat losses of the two pipes and the surface temperature contrast is also shown in Figure 8. The slope of the line defines the calibration constant of the simplified estimator (14). Comparison of the two graphs shows that (13) gives a significantly higher correlation than (14) for the near-stable conditions of t = 360 hours.

The algorithms discussed above are less well-defined over vegetation. The IR-temperature then highly depends on wind speed, plant height, air temperature, canopy density and transpiration rate [4]. For sparse vegetation, in particular, the observation angle has also an influence.

Similar to a dense canopy of vegetation, thick snow layers mask the temperature contrast of the heating line. The snow disappears faster, however, as a result of the increased melting rate. Hence, culverts with high energy losses give snow-free areas in the late winter season, which can easily be detected from visual inspection or aerial photography. The width of the snow-free area of the heating line is a non-linear function of the heat-losses, which also depends upon the preceding weather history and ground frost conditions.

When an IR-scanner is used for measurements of the ground surface temperature, the detected temperature contrast is attenuated by the intervening atmosphere. If we assume an atmospheric path transmission of 80 %, for instance, a thermal contrast of 5.0 K at ground will be detected as 4.0 K by the IR-sensor.

The temperature contrast is also reduced due to emissivity values below 1.0. More important, however, are the emissivity variations over inhomogeneous surfaces. Typically, $\Delta\varepsilon = 0.02$ changes the detected temperature about one degree at clear sky and 0.1 - 0.3 K at cloudy weather. A more detailed discussion on the emissivity and atmospheric effects can be found in [4]. Both types of errors can be compensated for, if the emissivity and sky temperature are predictable.

6 CONCLUSIONS

The analysis and simulation results show a strong correlation between the thermal-IR contrast of a district heating line and its heat losses. Simple algorithms were suggested for quantitative estimations of the energy losses based upon surface integration of the temperature anomaly.

A main-limitation at their application is the requirement of homogeneous ground conditions over the heating line area and the reference background. Differences in albedo, emissivity, surface humidity, thermal inertia, exposure for wind and radiation, for instance, will generate significant errors at the use of the algorithms. Their application is less reliable over surfaces covered by snow and vegetation and during the first days or week after a significant change of the insulation or water temperature.

In order to reduce the estimation error, the acquisition of IR-data should be performed during a period of calm weather and low solar radiation i.e. cloudy sky and the hours before dawn. Dry surface conditions and low air-temperatures will reduce the effects of varying evaporation but ground temperatures below 0°C should be avoided. The errors due to variations in emissivity and insolation are both minimized, if the IR-measurement is carried out below overcast sky.

ACKNOWLEDGEMENTS

This research was carried out at the University of Linköping with financial support from the Swedish Board for Space Activities. Thanks are also due to Mrs Ing-Marie Pilemalm for typing the manuscript.

REFERENCES

[1] R.J. Brown et al, Quantitative residential heat loss study, Photogr. Eng. Rem. Sens., pp 1327-33, 1981.

[2] H.W. MacKay, The application of airborne thermography for monitoring buried heat distribution lines, Proc. 8th Canad. Symp. Rem.Sens., 1984.

[3] S-Å Ljungberg, Airborne thermography - a tool for local energy planning (in Swedish). The National Swedish Institute for Building Research, Gävle, M:2, 1986.

[4] S.R.J. Axelsson, Thermal modeling for the estimation of energy losses from municipal heating networks using infrared thermography, Linköping University, LiTH-ISY-0814, 1986.

[5] J.A. Businger et al, Flux-profile relationships in the atmospheric surface layer, J.Atm.Sc.(28), pp 181-189, 1971.

[6] W. Brutsaert, Evaporation into atmosphere. D. Reidel Publ. Co., London, 1981.

[7] G.D. Smith, Numerical Solution of Partial Differential Equations. Oxford University Press, 1969.

[8] S.R.J. Axelsson, On the estimation of energy losses from municipal heating networks using infrared thermography, Proc. IGARSS'87, Ann Arbor, 18-21 May 1987.

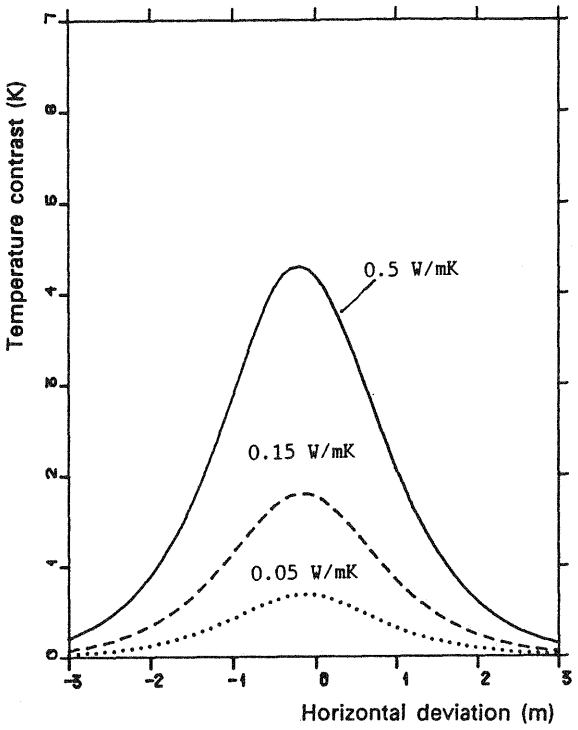

FIGURE 2. Temperature profiles versus insulation conductivity.

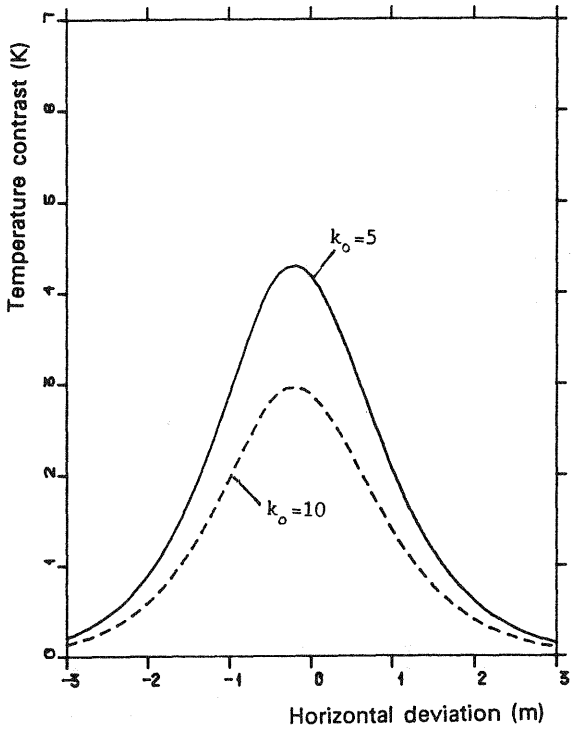

FIGURE 3. Temperature profiles for k_0=5 and 10 W/m^{2}K.

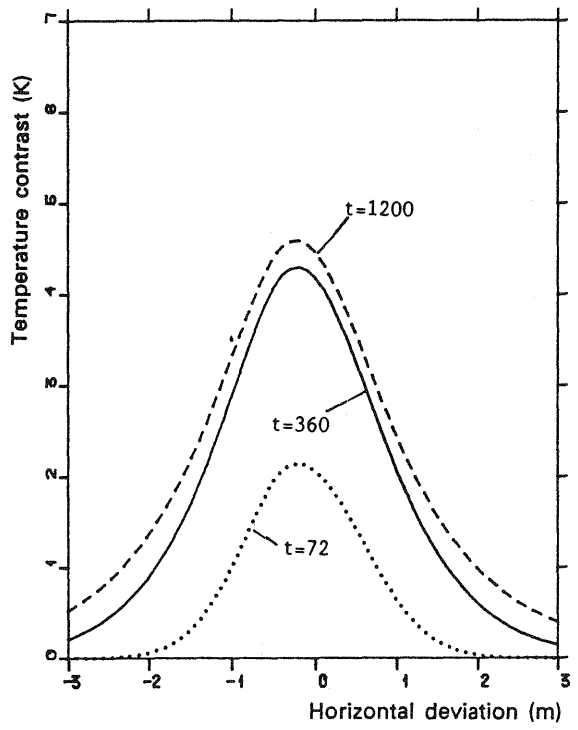

FIGURE 4. Temperature profiles for t=72, 360 and 1200 hours.

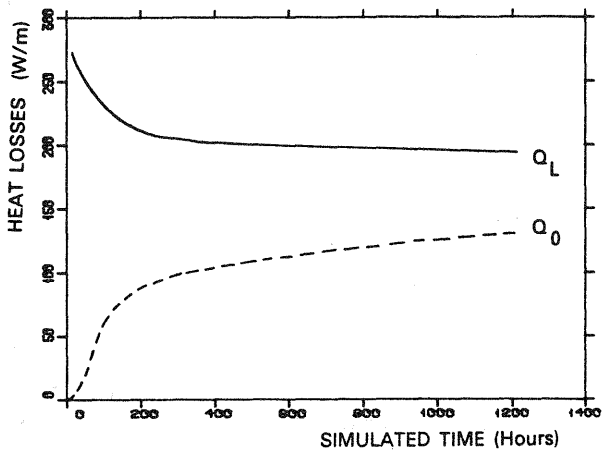

FIGURE 5. Time dependence of the total energy losses (Q_L) and the increased heat flux (ΔQ_0) at the surface.

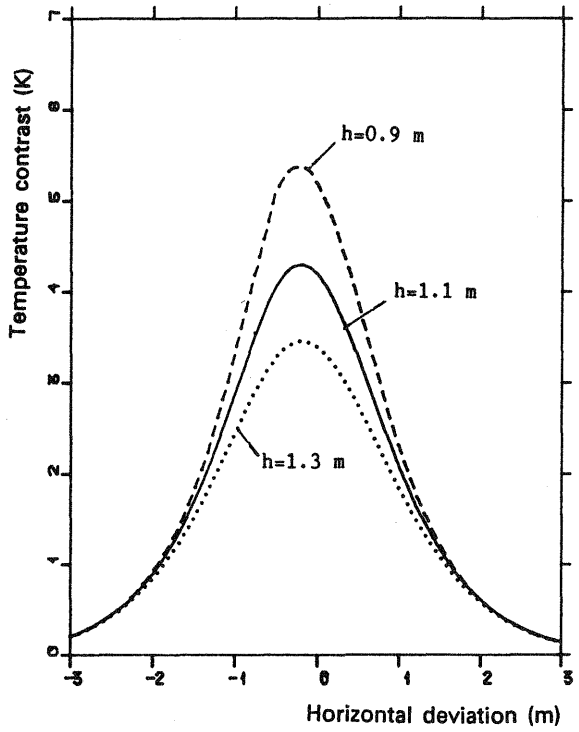

FIGURE 6. Temperature profiles for varying culvert depth.

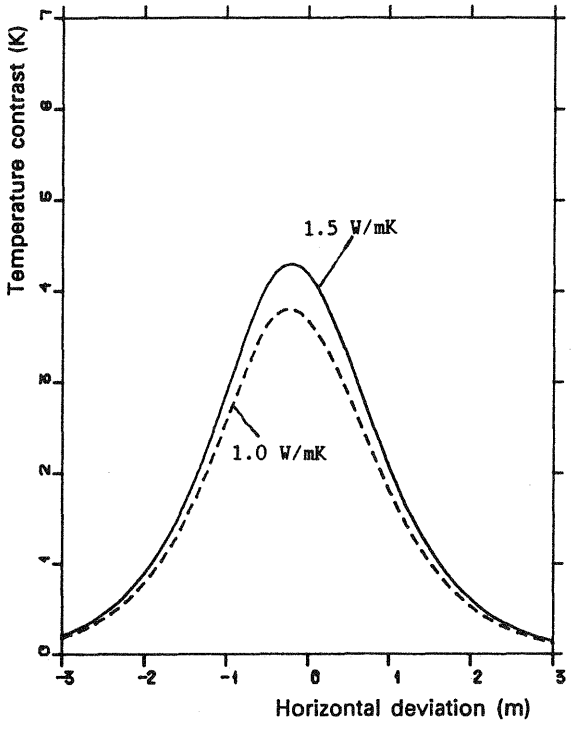

FIGURE 7. Dependence on the thermal soil conductivity (W/mK).

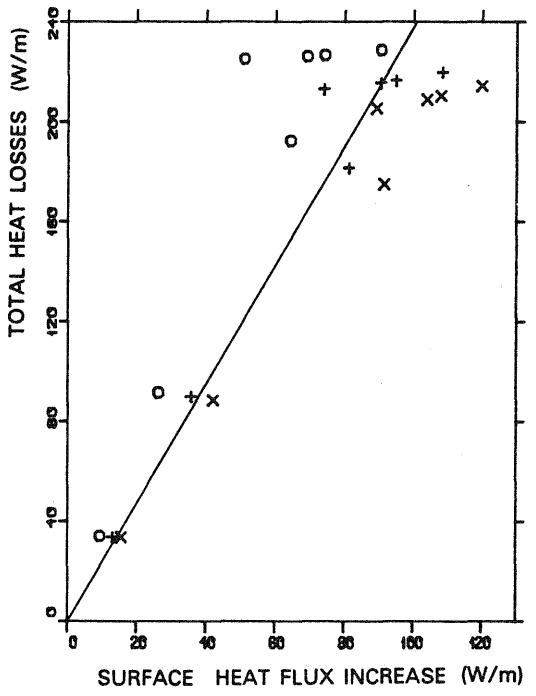

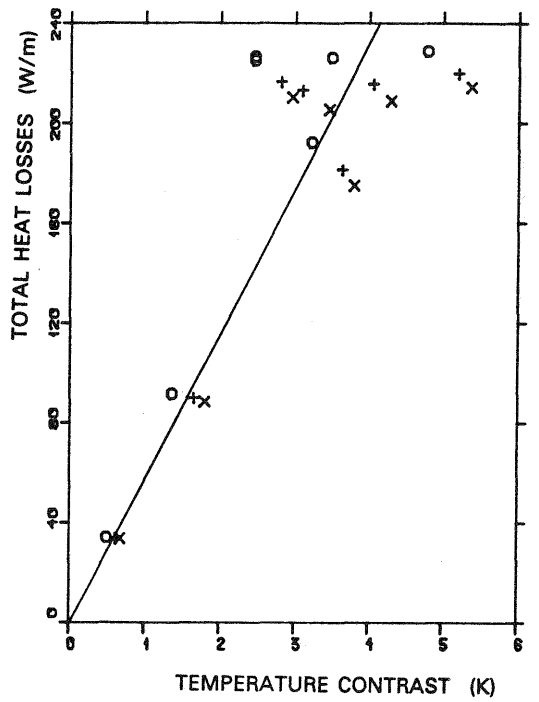

FIGURE 8. Total energy losses versus surface heat flux increase (left) and total energy losses versus temperature contrast at the surface (right). The relationships are predicted for the parameter choice of Figs. 2, 3, 6 and 7 with o = 144 hours, + = 240 hours and x = 360 hours.